Journal of Geophysical Research – Solid Earth

Supporting Information for

Stress balance in synthetic serpentinized peridotites deformed at subduction zone pressures

N. Hilairet[1], J. Guignard[2,*] , T. P. Ferrand[3, 4], S. Merkel[1], P. Raterron[1,**], B. Ildefonse[5], A. Fadel[6], W. Crichton[2]

1 : Univ. Lille, CNRS, INRAE, Centrale Lille, UMR 8207 - UMET - Unité Matériaux et Transformations, F-59000 Lille, France

2 : ESRF European Synchrotron, F-38000 Grenoble, France

*: now at IROX Technology, F-31104 Toulouse, France

3 : PSL Research University, Laboratoire de Geologie, Ecole Normale Superieure, CNRS UMR 8538, F-75005 Paris, France

4 : Institute of Geological Sciences, Freie Universität Berlin, Malteserstr. 74-100, 12249 Berlin, Germany

5 : Geosciences Montpellier, University of Montpellier, CNRS, Montpellier, France

6 : Univ. Lille, CNRS, INRAE, Centrale Lille, Université d'Artois, FR 2638 - IMEC - Institut Michel-Eugène Chevreul, F-59000 Lille, France

**now at : National Science Foundation, 2415 Eisenhower Avenue, Alexandria, Virginia 22314, USA

Contents of this file

Figures S1 to S8

Introduction

This file contains information about the high-pressure cell design (Figure S1), additional microstructural information for the recovered samples (figures S2 to S7), and further comparison of our results with the literature (Figure S8).

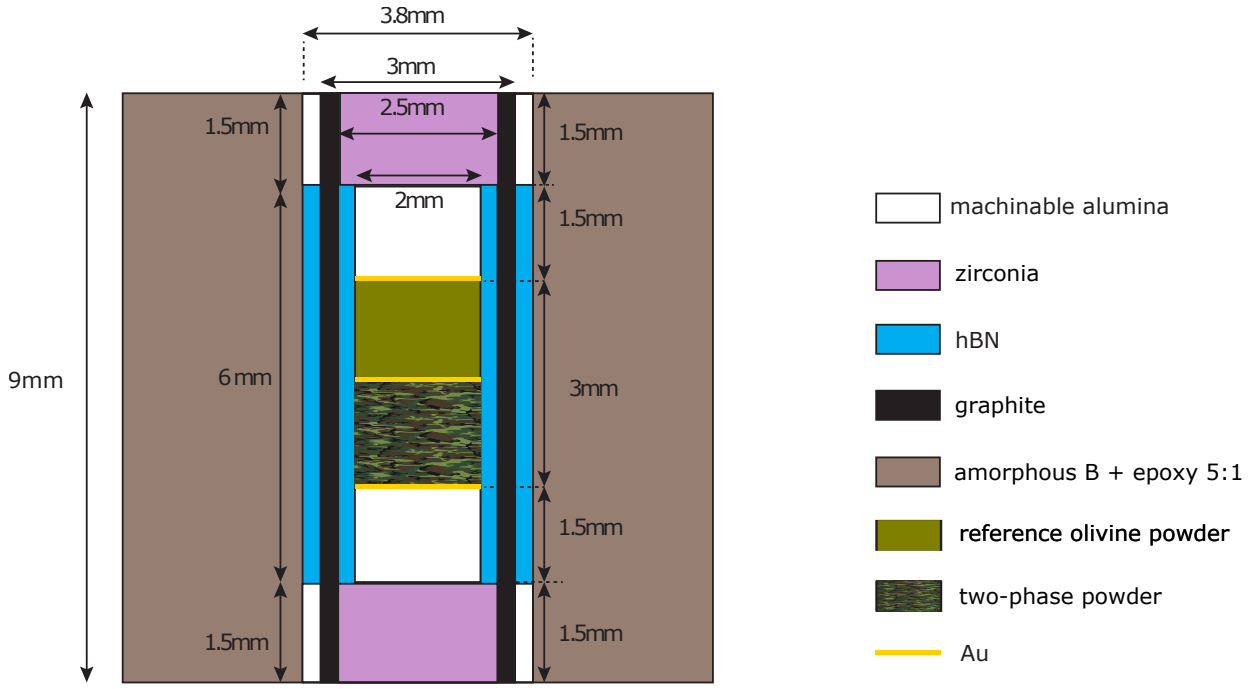

Figure S1. High-pressure cell design.

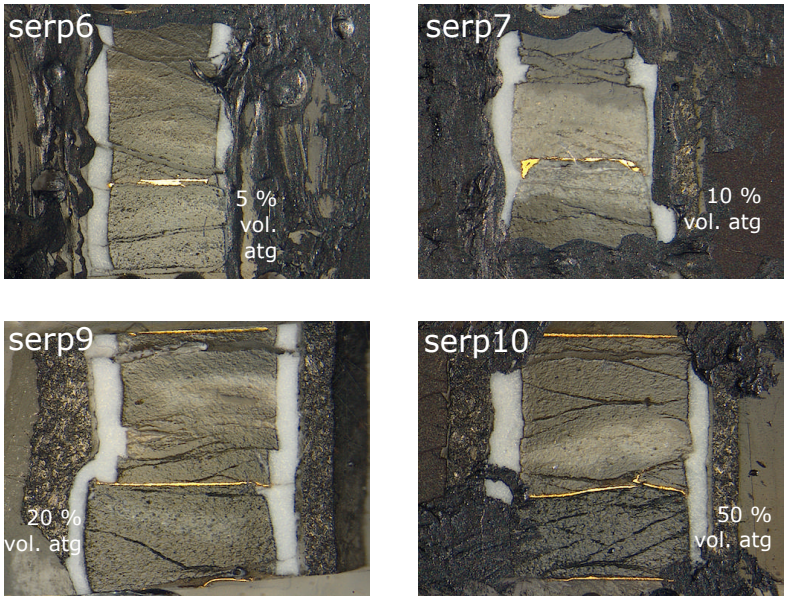

Figure S2. Micrographs of recovered samples. The two-phase aggregates parts are indicated by the proportion of antigorite in the aggregate. The samples are surrounded with conductive paste for electron microscopy analysis.

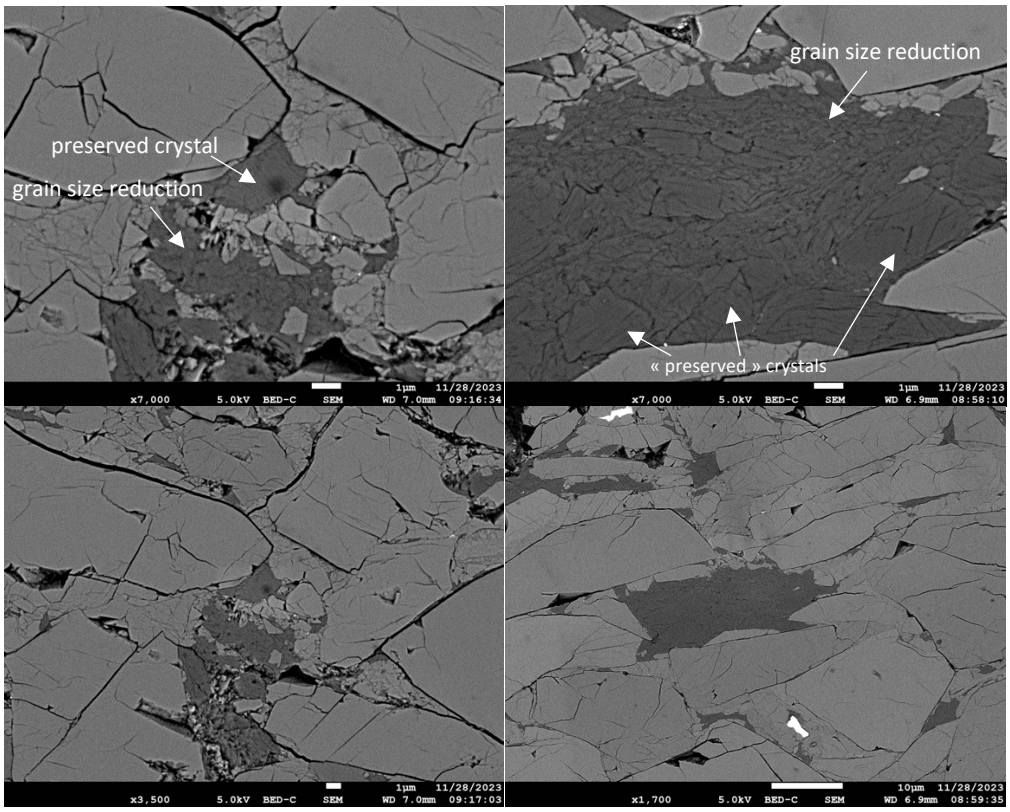

Figure S3. Microstructures in antigorite as seen by BSE (darker grey is antigorite, lighter gray is olivine, rare bright crystals are oxydes), for the samples recovered from run serp6 (images on the left) and serp7 (on the right). The images at the top show preservation of some large crystals of antigorite and grain size reduction to submicron sizes. The images at the bottom are larger views of the same area, showing microcracking of olivine at the *crystal* scale.

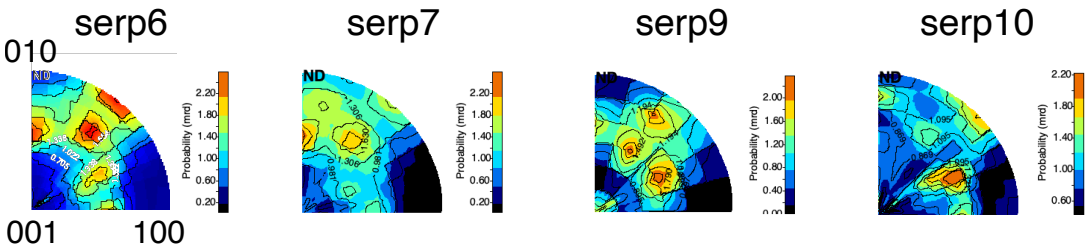

Figure S4. The starting LPO (lattice preferred orientations) of olivine have been retrieved from in situ diffraction analysis on the two-phase aggregates taken under pressure and temperature, and before deformation, using the MAUD software (Lutterotti et al. 2007).
They are presented as inverse pole figures for the maximum compression direction, in multiples of random deviation (1 = random).
The features are at very first order similar for all samples after pressurization, with a strong minimum probability of having the a axes along the compression direction. With some variability between the samples, minima are also found for b and c axes.
A qualitative comparison with figure 5 shows that deformation induced, in all two-phase samples, rotation of the b axes and a axes closer to the maximum compression direction.

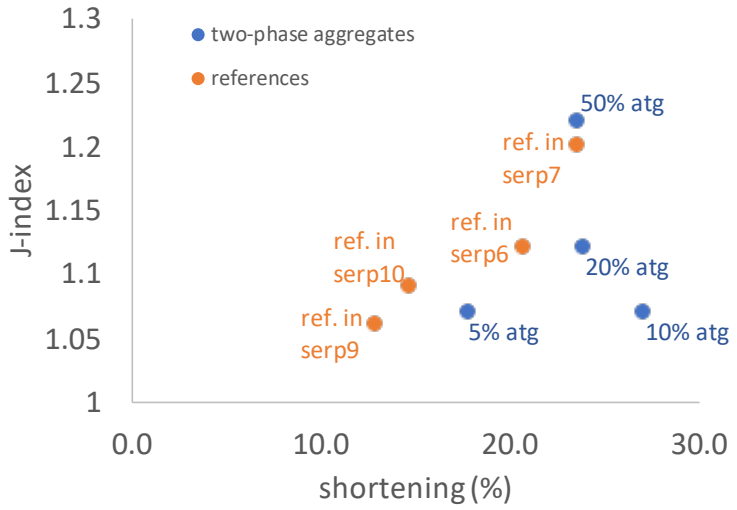

Figure S5. J-index (Bunge, 1982) of CPO from EBSD measurements on recovered samples. For olivine in 5 and 10 vol. % serpentine aggregates, the J-index is 1.07 and increases to 1.12 for 20 vol. % of serpentine. The 5 vol % atg. aggregate compared to the reference olivine aggregate deformed under the same P and T, at a similar amount of strain (19 vs. 21% strain), shows a weaker CPO. The 20 vol. % serpentine aggregate, deformed up to 24% strain, shows a slightly weaker CPO than its reference olivine counterpart deformed only to 13% axial strain.

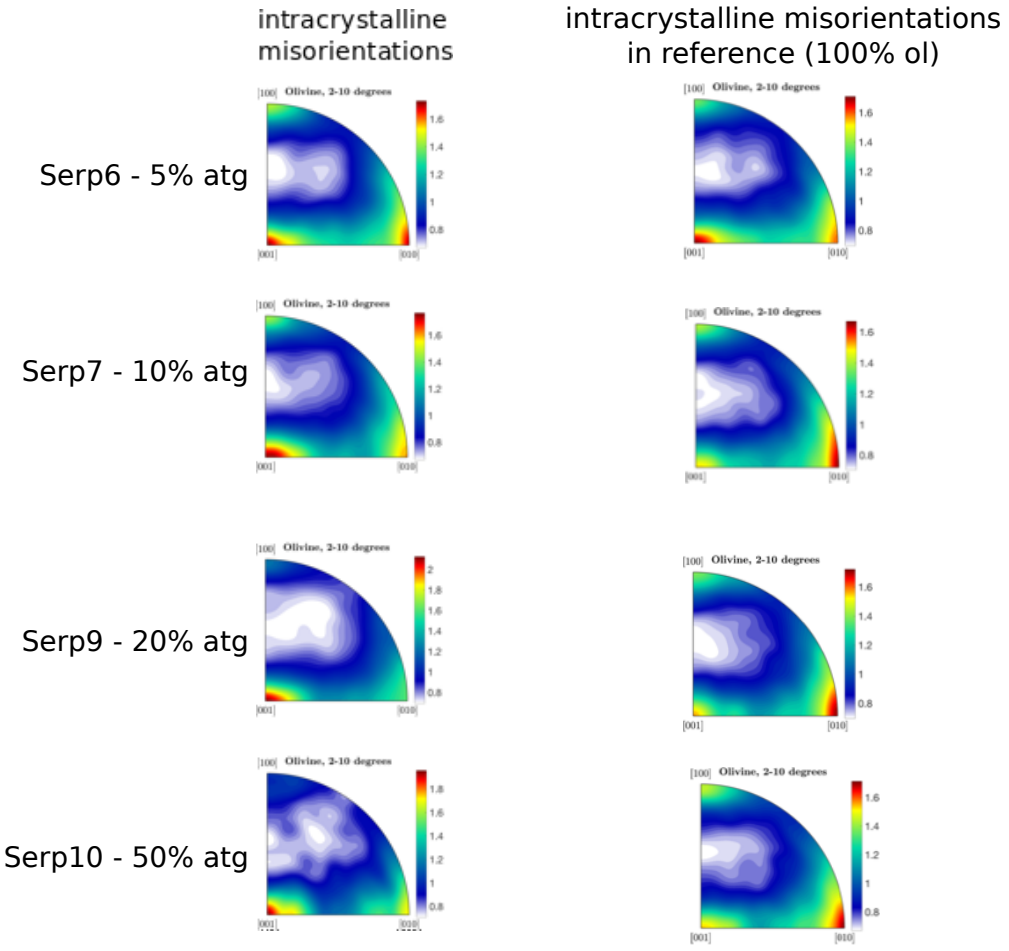

Figure S6. Inverse pole figures for misorientation rotation axes, for low angle grain boundaries (2°-10°) in olivine.

Interpretation: The misorientation analysis for low-angle grain boundaries (2-10°) appears here as the best way to examine the slip systems at play for intracrystalline plasticity in olivine grains. In all samples, the strongest maxima are generally seen along [001] and [010]. A secondary maximum around [100] appears for low antigorite volume contents and reference aggregates with no antigorite. These strongest maxima around 010 and 001 poles correspond to rotation axes accommodating misorientations parallel to [010] and [001]. At first order, following relationships outlined by Lloyd et al. (1998), (001)[100], (100)[001], and (010)[100] slip systems correspond to these orientations. The secondary maximum around [100] for low antigorite volume contents (5 and 10 vol. %) and 100% olivine aggregates could correspond to activation of the (010)[001] slip system at higher stresses either locally and/or globally.

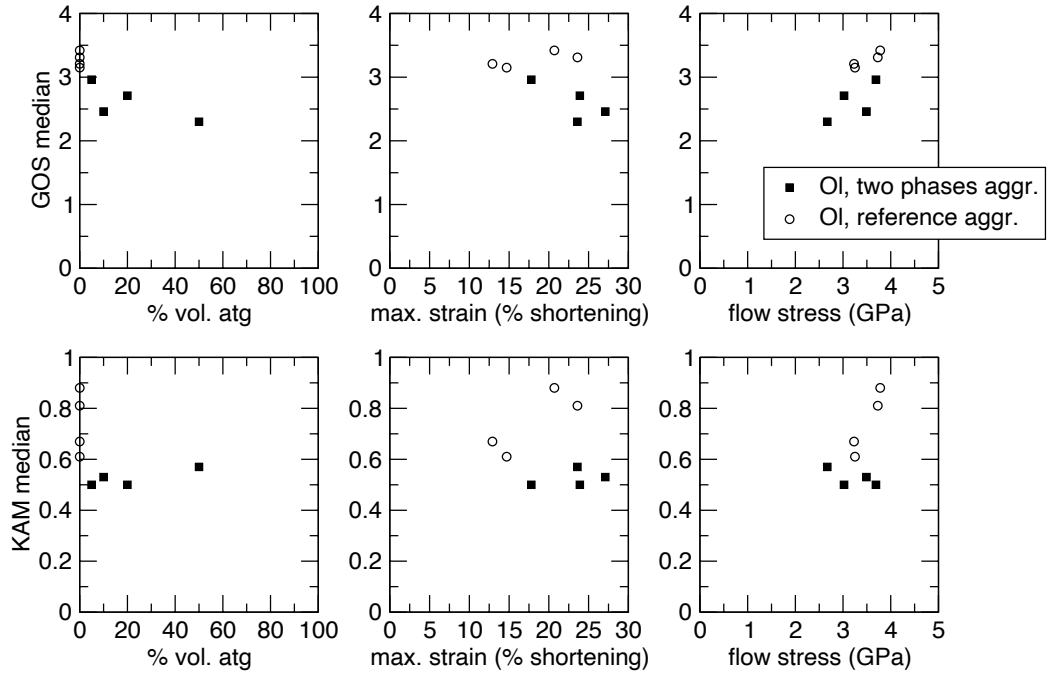

Figure S7. Median KAM and GOS values as a function of stress, final strain and atg vol. fraction in the aggregate.

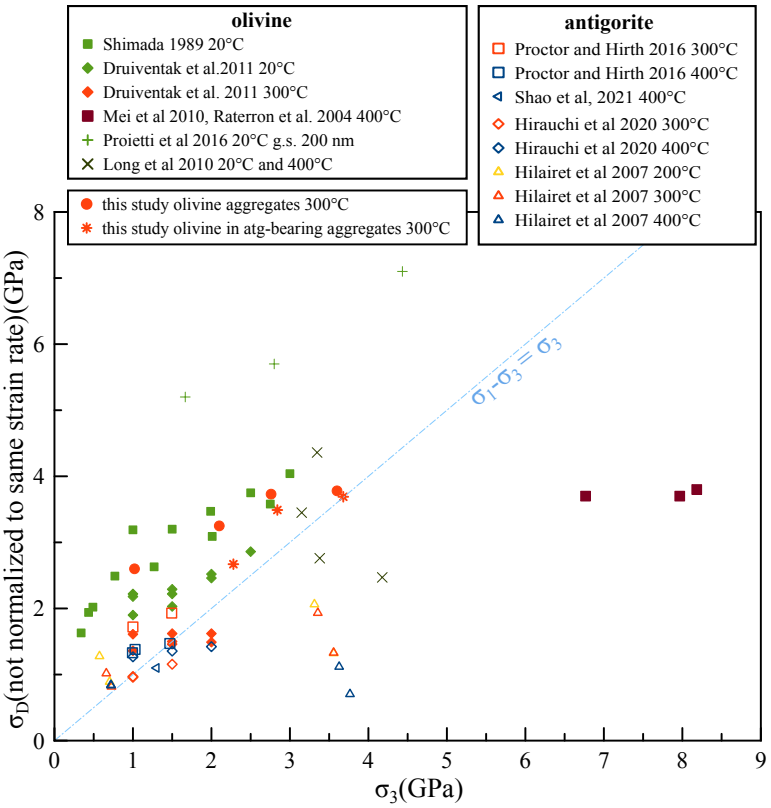

Figure S8. Differential stress vs. pressure for antigorite+olivine aggregates and for olivine and antigorite aggregates from the literature. Note the amount of total strain reached and the mean stress in these data is diverse. The values for σ_D (i.e. σ_1-σ_3) are not normalized to the same pressure, temperature or strain rate.

Discussion on figure S8.

For olivine, data that were obtained between room T to 400°C (Druiventak et al, 2011; Long et al, 2010; Proietti et al, 2016) are used. Other data on olivine (Mei et al, 2010; Raterron et al, 2004) fall well below the Goetze criterion, and are less relevant for comparisons. Druiventak et al. (2011) stress levels on natural peridotites fall below those measured in the other studies. Their experiments have been conducted on natural samples with pyroxene as secondary phases (lower than 5 and 10% depending on the starting material), and larger grain sizes than the present experiments (100s of microns while ours are ca. 1 up to 40 microns), that could partly explain the discrepancies. Finally, the temperature during the course of our DDIA experiments can be overestimated, as explained in the methods section.

The results of Proietti et al (2016) at ambient T, on polycrystalline olivine show a similar trend but plot about 2 GPa above the others. The starting grain size (ca. 200 nm) may be responsible for this difference, as aggregates with sub-micron grain size could have different mechanical properties. Again, our data for reference aggregates are well within the trend for olivine aggregates under increasing pressure.

For antigorite-bearing aggregates our data are closer to the Goetze criterion but remain well above the values for pure antigorite aggregates taken from the literature,

under similar pressure and temperature conditions, except for the aggregate at 50% vol. antigorite which may be seen as extending the data on pure antigorite by Proctor and Hirth (2016).

References:

Druiventak, A., Trepmann, C.A., Renner, J., Hanke, K. (2011). Low-temperature plasticity of olivine during high stress deformation of peridotite at lithospheric conditions — An experimental study. *Earth and Planetary Science Letters 311*, 199-211, doi: https://doi.org/10.1016/j.epsl.2011.09.022.

Lloyd, G. E., Farmer, A. B., Mainprice, D. (1997) Misorientation analysis and the formation and orientation of subgrain and grain boundaries, *Tectonophysics*, 279, 1-4, 55-78, doi: 10.1016/S0040-1951(97)00115-7

Long, H., Weidner, D.J., Li, L., Chen, J., Wang, L. (2011). Deformation of olivine at subduction zone conditions determined from in situ measurements with synchrotron radiation. Physics of the Earth and Planetary Interiors 186, 23-35, doi: 10.1016/j.pepi.2011.02.006.

Lutterotti, L., Bortolotti, M., Ischia, G., Lonardelli, I., Wenk, H.-R. (2007). Rietveld texture analysis from diffraction images. Z Kristallogr. Suppl. (Suppl 26), 125–130, doi: 10.1524/zksu.2007.2007.suppl_26.125

Mei, S., Suzuki, A.M., Kohlstedt, D.L., Dixon, N.A., Durham, W.B. (2010). Experimental constraints on the strength of the lithospheric mantle. Journal of Geophysiscal Research 115, B08204, doi: 10.1029/2009jb006873.

Proctor, B., Hirth, G. (2016). "Ductile to brittle" transition in thermally stable antigorite gouge at mantle pressures. Journal of Geophysical Research-Solid Earth 121, 1652-1663, doi: 10.1002/2015jb012710.

Proietti, A., Bystricky, M., Guignard, J., Béjina, F., Crichton, W. (2016). Effect of pressure on the strength of olivine at room temperature. Physics of the Earth and Planetary Interiors 259, 34-44, doi: https://doi.org/10.1016/j.pepi.2016.08.004.

Raterron, P., Wu, Y., Weidner, D.J., Chen, J. (2004). Low-temperature olivine rheology at high pressure. Physics of The Earth and Planetary Interiors 145, 149, doi: 10.1016/j.pepi.2004.03.007